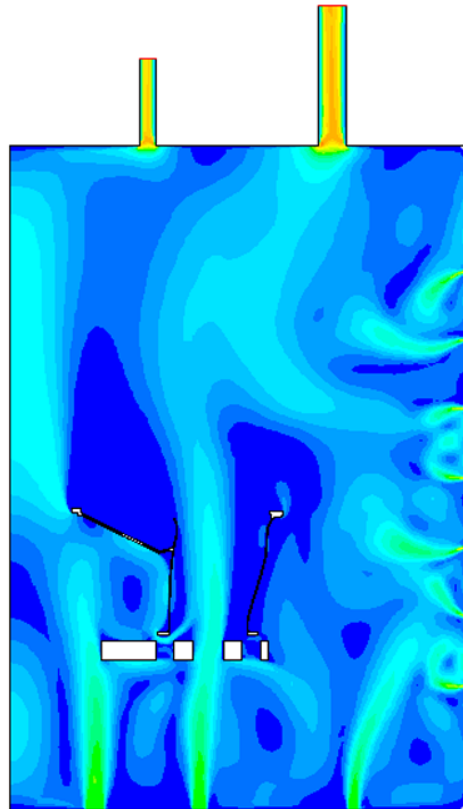# CHALMERS

CFD Heat Transfer Validation of Turbine Structure Heat Treatment Process

Master's Thesis in Solid and Fluid Mechanics

EMIL BERGMAN

CFD Heat Transfer Validation of Turbine Structure Heat Treatment Process

Master's Thesis in Solid and Fluid Mechanics
EMIL BERGMAN

Department of Applied Mechanics
Division of Fluid Mechanics
CHALMERS UNIVERSITY OF TECHNOLOGY

Göteborg, Sweden 2012

CFD Heat Transfer Validation of Turbine Structure Heat Treatment Process
EMIL BERGMAN

Cover:
Velocity magnitude of a 2D axi-symmetric heat transfer simulations

CFD Heat Transfer Validation of Turbine Structure Heat Treatment Process
Master's Thesis in Solid and Fluid Mechanics
EMIL BERGMAN
Department of Applied Mechanics
Division of Fluid Mechanics
Chalmers University of Technology

Abstract

Volvo Aero Corporation is a subcontractor that mainly delivers structural components to both civil and military jet-engines for several large jet-engine manufacturers such as General Electrics, Pratt & Whitney and Rolls-Royce. One of these components is the Turbine Rear Structure (TRS) which has the main purpose of supporting the engine core.

The TRS is fabricated from a combination of cast metal, sheet metal and machined metal parts. During the manufacturing process it undergoes a precipitation hardening process which is a two stage process where the first stage is a so called solution heat treatment and the second stage is the precipitation hardening. During solution heat treatment, the material temperature is slowly increased and held there until the material temperature is suddenly dropped resulting in a very aggressive cooling. This aggressive cooling gives a very non-uniform cooling rate of the component which in turn creates large thermal stresses and finally damage the component.

The purpose of this thesis is therefore to, by CFD simulations, obtain a deeper understanding of the heat treatment process and its problems with large thermal stresses. The thesis goal is to establish a methodology for how to tackle similar problems in the future.

The thesis methodology was first to investigate how well heat transfer can be predicted for different reference cases and then try to simulate the precipitation hardening process using CFD. A pre-study was made for three cases, flow past flat plate, flow through a ribbed channel and flow past a 2D cylinder. The main results from these simulations show that the heat transfer rate can be predicted quite well as long as the turbulence intensity is not too great.

The main study was performed in two steps. First a 2D axi-symmetric model of the process was simulated where the results showed that radiation is crucial for the overall heat transfer meanwhile the convective heat transfer mainly contributes to local temperature variations.

In reality however the flow pattern is very complex and cannot be simplified into a 2D axi-symmetric case. 3D simulations are therefore needed. However due to lack of time and knowledge about mesh generation 3D simulations was never carried out.

The final conclusions is that despite that 3D simulations was never performed, the heat treatment process can be simulated. However it will be a very large simulation including all heat transfer phenomena's.

Keywords: Heat transfer, Precipitation hardening, Cooling, CFD, Turbine Rear Structure, Flat plate, Ribbed channel, Cylinder in cross flow

Contents

Preface

The Master thesis presented in this report was performed during the spring of 2012 as a final part of the Master Programme in Solid and Fluid Mechanics at Chalmers University of Technology in Göteborg, Sweden. The thesis was approved by the Division of Fluid Dynamics at the Department of Applied Mechanics at Chalmers University of Technology. The work has been carried out for the department for Aerothermodynamics at Volvo Aero Corporation in Trollhättan, Sweden. The thesis have been supervised by Andreas Fahlvik Svensson and Hans Abrahamsson at Volvo Aero Corporation and Ph. D. Niklas Andersson at Chalmers University of Technology has been the thesis examiner.

Aknowledgements

I like to thank my supervisors Hans Abrahamsson and Andreas Fahlvik Svensson for the opportunity and for showing great interest and appreciation in the project. I would also like to thank all my colleagues at Volvo Aero Corporation for having made my time at Volvo Aero great. My master theses colleague Gustav Johansson also deserves my gratitudes for not only been my friend but also for serving as a sounding board throughout the whole project. Last I like to thank my supervisor Niklas Andersson for the support and for making this thesis run smoothly.

Göteborg May 2012
Emil Bergman

Nomenclature

Greek symbols

α, α_t Thermal diffusivity, turbulence thermal diffusivity

δ_{ij} Kronecker delta

μ, μ_t Dynamic viscosity, turbulence dynamic viscosity

ν, ν_t Kinematic viscosity, turbulence kinematic viscosity

ω Specific dissipation rate of turbulence kinetic energy

Φ Viscous dissipation

ρ Density

σ, σ_θ Stefan-Boltzmann constant, turbulent Prandtl number

θ Temperature

ε Dissipation of turbulence kinetic energy, material emissivity

Latin symbols

$\dot{m}$ Mass flow rate

b Buoyancy

C_p Specific heat capacity

i Internal energy

k Turbulence kinetic energy, thermal conductivity

L_c Characteristic length

P Pressure

P_k Production of turbulence kinetic energy

q'' Heat flux

u Velocity

A   Area

h   Convective heat transfer coefficient

L   Length of plate

T   Temperature

t   Time

x   Spatial coordinate, distance

Subscripts

b   Bulk property

conv   Convective

f   Fluid property

rad   Radiative

s   Surface property

sur   Surrounding

Acronyms

Bi Biot number

CFD Computational Fluid Dynamics

Fo Fourier number

HTC Heat Transfer Coefficient

LCM, GLCM Lumped Capacitance Method, General Lumped Capacitance Method

Nu Nusselt number

Pr Prandtl number

Ra Rayleigh number

Re Reynolds number

SST Shear Stress Transport model

TRS Turbine Rear Structure

1 Introduction

This chapter gives an introduction to the project. It contains a short background, purpose, problem description and limitations.

1.1 Background

Volvo Aero is a subcontractor that mainly manufactures and develops structural components for a variety of commercial and military jet-engines. One of these components is the Turbine Rear Structure (TRS). The TRS is a load carrying structural component located aft of both the combustor and the low pressure turbine (LPT). Its purpose is to support the engine core and redirect the exhausts in a pure axial direction. Figure 1.1 shows a typical turbofan engine and its main parts, Fan, Low Pressure Compressor or Booster (LPC), High Pressure Compressor (HPC), Combustor Chamber (CC), High Pressure Turbine (HPT), Low Pressure Turbine (LPT) and Turbine Rear Structure (TRS). The TRS is a complex component that withstands heavy loadings
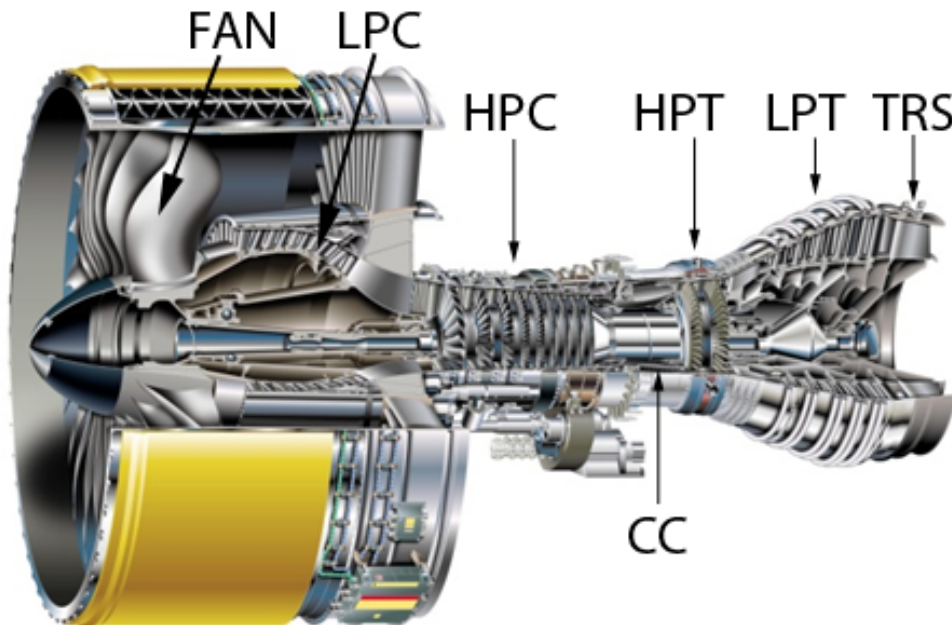

Figure 1.1: Typical turbofan engine

for a long time at an elevated temperature. Due to this the TRS is a critical component of the turbofan jet engine that has to fulfil very high requirements on strength. Since its a stationary load baring component it is also a relatively heavy component that if it could be designed in a more optimal way, the overall engine weight will decrease and ultimately result in lower fuel consumption. Volvo Aero have therefor developed the TRS, studied in this thesis, so that it is lighter than its predecessor but still fulfills the requirements. However it has been shown that the component complexity have created some problems during the manufacturing process and especially the heat treatment process where large thermal stresses damage the component.

During manufacturing the component undergoes a number of heat treatments with the purpose of improving the structural properties and to lower

internal stresses induced by weldings. The heat treatment process studied within this thesis is called precipitation hardening process. It is a two stage process that consist of a solution heat treatment and then a precipitation hardening.

In the heat treatment process the temperature of the component is slowly elevated to a suitable value and then rapidly cooled again. It is essential that the cooling part of the process is done as isothermal as possible to avoid large thermal stresses that might damage the component and create small cracks. This is a great problem since these cracks have to be repaired by welding which in turn alters the material properties and the component needs to be heat treated again resulting in a never ending repair loop.

1.2 Purpose

The purpose of this project is to obtain a deeper understanding of the heat transfer problem during the aggressive cooling part of the precipitation hardening and to evaluate the possibility of performing CFD simulations in order to estimate the location of thermal stresses induced by large thermal gradients.

1.3 Problem description

A deeper understanding of the heat transfer problem that occurs during the aggressive cooling of the solution heat treatment is obtained by CFD simulations for three reference cases. Also strengths and weaknesses of the CFD tools are identified by doing a simulation with flow conditions corresponding t those in the heat treatment process.

1.4 Limitations

The thesis consists of three pre-study reference cases where CFD tools and heat transfer phenomenas are studied. These reference cases are; flow past a flat 2D plate, flow through a ribbed channel and flow past a 2D cylinder. The results are then compared and analysed with well-recognised heat transfer correlations. In the ribbed channel case the results are compared with experimental studies. The studied methods are:

- Laminar flow simulation

- Turbulence models

  - Realisable k-ε
  - SST k-ω

- Transient vs. Quasi-Transient heat transfer simulations

- Fluid-Solid thermal coupling

The main part consists of CFD simulations of first a 2D axi-symmetric model of the solution heat treatment part, including the oven geometry, the TRS

and the graphite plate which it is standing on. However the model has been simplified a bit. A large complex steel structure underneath the graphite plate have been disregarded in order to simplify the mesh generation and flow pattern. More detail about the simplifications made can be found in section 3.3.

2 Theory

This section provides basic theory that the thesis is built upon. First the governing equations for fluid flow and energy transportation are presented. Then some basic theory about turbulence modelling and precipitation hardening followed by a short review of the heat transfer properties used later in the project.

2.1 Governing equations

The governing equations used for calculating the fluid flow pattern and energy transportation are [8]:

$$\frac{\partial \rho}{\partial t} + \frac{\partial(\rho u_i)}{\partial x_i} = 0 \tag{2.1}$$

$$\frac{\partial \rho u_i}{\partial t} + \frac{\partial(\rho u_i u_j)}{\partial x_j} = -\frac{\partial P}{\partial x_i} + \mu \frac{\partial^2 u_i}{\partial x_j} + \rho b_i \tag{2.2}$$

$$\frac{\partial \rho i}{\partial t} + \frac{\partial(\rho i u_i)}{\partial x_j} = -P \frac{\partial u_i}{\partial x_j} + \frac{\partial}{\partial x_j}\left(k \frac{\partial \theta}{\partial x_i}\right) + \Phi \tag{2.3}$$

Where ρ, u_i, p, b_i, i, k, θ and Φ denotes density, velocity, pressure, buoyancy, internal energy, thermal conductivity, temperature and viscous dissipation, respectively. Equation (2.1) is known as the continuity equation which states that mass is conserved. Equation (2.2) is the Navier-Stokes equations which describes transportation of momentum. Finally, equation (2.3) is called the energy equation which describes transportation of energy within the fluid. Since these equations are highly complex and non-linear they can only be solved analytically for a small number of very simple cases. These simple cases are however very rare in reality and can therefore very seldom be applied. Instead the equations are solved numerically for a discrete flow domain.

2.2 Turbulence modelling

In general almost all fluid flow problems that one encounter as an engineer are turbulent. Meaning that the flow pattern have chaotic fluctuations with a vast variety of time and length scales. Solving a turbulent flow case exactly is therefore very computationally demanding since the resolution of the discretisation, both spatially and temporal, needs to be extremely high in order to capture even the smallest length and time scales. A less expensive method is, instead of solving the governing equations for the instantaneous flow field, to solve the time-averaged Navier-Stokes equations governing the mean flow. These equations are derived by first decomposing the instantaneous flow field into a mean and a fluctuating part which then are time-averaged. Equation

(2.4) shows the decomposed velocity components where the $\bar{\cdot}$ denotes time averaged values.

$$u_i = \bar{u}_i + u_i' \tag{2.4}$$

Excluding the energy equation for now the time averaged continuity and Navier-Stokes equations for steady state, incompressible flow with constant viscosity and zero gravity are shown below as stated in [2].

$$\frac{\partial \bar{u}_i}{\partial x_i} = 0 \tag{2.5}$$

$$\rho \frac{\partial \bar{u}_i \bar{u}_j}{\partial x_j} = -\frac{\partial \bar{p}}{\partial x_i} + \frac{\partial}{\partial x_j} \left(\mu \frac{\partial \bar{u}_i}{\partial x_j} - \rho \overline{u_i' u_j'} \right) \tag{2.6}$$

These equations contains mostly mean variables however to the far right of equation (2.6) new terms have arisen. These are the time-averaged velocity fluctuations and are called Reynolds stresses. The Reynolds stresses adds another six unknown variables to the previous four. Since there are only four equations and ten unknowns six more equations are needed in order to close the equation system. The most widely used way for doing so is to use the Boussinesq assumption. The Boussinesq assumption is a simplification that replaces the six turbulent stresses with one new unknown variable, the turbulent viscosity (ν_t). It can be compared to the fluid viscosity but a property of the flow rather than a fluid property like the ordinary viscosity. Boussinesqs assumption models the turbulent stresses as

$$\overline{u_i' u_j'} = -\nu_t \left(\frac{\partial \bar{u}_i}{\partial x_j} + \frac{\partial \bar{u}_j}{\partial x_i} \right) + \frac{2}{3} \delta_{ij} k \tag{2.7}$$

For the energy equation a similar expression for the heat flux vector, $\overline{u_i' \theta'}$, reads

$$\overline{u_i' \theta'} = -\alpha_t \frac{\partial \bar{\theta}}{\partial x_i} \tag{2.8}$$

Where α_t is defined as

$$\alpha_t = \frac{\nu_t}{\sigma_\theta} \tag{2.9}$$

and σ_θ is the turbulent Prandtl number, usually set to $0.7 \leq \sigma_\theta \leq 0.9$.

After simplifying the equation system using Boussinesq assumption we now have five unknown variables but still only four equations, one more equation that models the turbulence viscosity is therefore needed. Modelling this can be done in several ways, each with its own strengths and weaknesses.

The simplest way of modelling the turbulence viscosity is to model it with equation (2.10) that uses the turbulence kinetic energy, k, and turbulence dissipation rate, ε, to calculate ν_t.

$$\nu_t = c_\mu \frac{k^2}{\varepsilon} \tag{2.10}$$

The turbulence kinetic energy, k, is the sum of all normal Reynolds stresses and ε is the dissipation of turbulence kinetic energy. Below follows how the turbulence models used in this thesis models the turbulence kinetic energy and the turbulence dissipation rate.

2.2.1 The realisable k-ε model

As mentioned before one of the eddy-viscosity models used during this project is the realisable k-ε model. It is based on the standard k-ε model which can be found in [2], however it has been modified to fulfil the realizability constraints that prevents the model from obtaining unphysical results during certain turbulent flow cases. In the realisable k-ε model the eddy-viscosity is modelled as equation (2.11)

$$\nu_t = \rho C_\mu \frac{k^2}{\varepsilon} \tag{2.11}$$

Where C_μ is a variable dependent on the flow.

The k- and ε-equations for the realisable k-ε model as stated in [7] are shown in equation (2.12) and (2.13), respectively.

$$\frac{\partial \rho k}{\partial t} + \frac{\partial \rho k u_j}{\partial x_j} = \frac{\partial}{\partial x_j}\left[\left(\mu + \frac{\mu_t}{\sigma_k}\right)\frac{\partial k}{\partial x_j}\right] + P_k - \rho\varepsilon \tag{2.12}$$

$$\frac{\partial \rho\varepsilon}{\partial t} + \frac{\partial \rho\varepsilon u_j}{\partial x_j} = \frac{\partial}{\partial x_j}\left[\left(\mu + \frac{\mu_t}{\sigma_\varepsilon}\right)\frac{\partial \varepsilon}{\partial x_j}\right] + C_1\rho S\varepsilon - C_2\rho\frac{\varepsilon^2}{k + \sqrt{v\varepsilon}} \tag{2.13}$$

2.2.2 The SST k-ω model

The other eddy-viscosity model utilised is the SST k-ω model brought forward by F.R. Menter [6]. It is a combination of the standard k-ε model and the k-ω model where the last one is used for the inner region of the boundary layer and the k-ε model for the rest of the flow field. The eddy-viscosity model is stated as equation (2.14)

$$\nu_t = \frac{a_1 k}{max(a_1\omega;\ \Omega F_2)} \tag{2.14}$$

Where the denominator takes the maximum of production and dissipation of turbulent kinetic energy, ω. Further derivation of the eddy-viscosity model can be found in [6].

The k-ω model is better in near wall regions than the k-ε model which is simpler to use further out from the wall. The SST k-ω model uses the advantages of both models and can therefore be used for a wider range of flow cases. The k- and ω-equation as stated in [6] are presented by equation (2.15) and (2.16), respectively.

$$\frac{D\rho k}{Dt} = \tau_{ij}\frac{\partial u_i}{\partial x_j} - \beta^*\rho\omega k + \frac{\partial}{\partial x_j}\left[(\mu + \sigma_k\mu_t)\frac{\partial k}{\partial x_j}\right] \tag{2.15}$$

$$\frac{D\rho\omega}{Dt} = \frac{\gamma}{\nu_t}\tau_{ij}\frac{\partial u_i}{\partial x_j} - \beta\rho\omega^2 + \frac{\partial}{\partial x_j}\left[(\mu + \sigma_\omega\mu_t)\frac{\partial \omega}{\partial x_j}\right] \tag{2.16}$$

2.3 Heat transfer

During the project, all heat transfer phenomenas, conduction, convection and radiation, are accounted for. However the conductivity heat transfer for fluid flow is much less than the convective and radiative heat transferwhich is why it will not be studied closer.

When studying the convective heat transfer the convective heat transfer coefficient (HTC) is often used. It is a coefficient that describes the amount of heat transferred across a wall in relation to the wall and fluid bulk temperature difference. Equation (2.17) shows the definition of the HTC value as it is stated in [5].

$$HTC = \frac{q''_{conv}}{T_s - T_b} \tag{2.17}$$

Where q''_{conv}, T_s and T_b are the convective heat flux, surface temperature and fluid bulk temperature, respectively. The fluid bulk temperature is the mean temperature of the bulky flow, i.e. local temperature differences due to boundaries are not included. For one of the pre-study cases the results where compared to experiments where the bulk temperature increased along the channel. For this case the bulk temperature was estimated according to equation (2.18)

$$T_b = T_{in} + \frac{q''_{conv} A \left(x/L \right)}{\dot{m} C_p} \tag{2.18}$$

Where the T_{in} is the temperature at the beginning of the heated section, A the heated plate area, $\dot{m}$ and C_p is the mass flow rate and specific heat, respectively.

Another very useful value is the Nusselt number (2.19). The Nusselt number describes the relation between convection and conduction, [5].

$$Nu = \frac{hL}{k_f} \tag{2.19}$$

Where h, L and k_f are HTC, surface length and fluid conductivity, respectively.

Radiation on the other hand is a heat transfer phenomena that transfers heat due to electro magnetic radiation and it is defined as (2.20)

$$q''_{rad} = \varepsilon \sigma \left(T_s^4 - T_{sur}^4 \right) \tag{2.20}$$

Where ε, σ, T_s and T_{sur} is the material emissivity, Stefan-Boltzmann constant, surface temperature and surrounding surface temperature, respectively.

During one of the pre-study cases the fluid-solid coupling is evaluated. Which means that also the material temperature of the solid is calculated. There are two ways of doing this analytically. These methods are called the Lumped Capacitance Method (LCM) and the General Lumped Capacitance method (GLCM). The difference between these two methods are that the Lumped method assumes that the temperature is spatially uniform during heating or cooling meanwhile the General Lumped method does not. The Lumped Capacitance Method calculates the material temperature using equation (2.21)

$$\frac{T_1 - T_2}{T_2 - T_\infty} = \frac{hL_c}{k} \equiv Bi \tag{2.21}$$

Where T_1, T_2, T_∞, h, L_c, k and Bi are the initial temperature, material temperature, bulk temperature, heat transfer coefficient, characteristic length, conductivity and Biot number, respectively. The characteristic length is

usually defined as the ration between the solid's volume and surface area. The Biot number, Bi, is a non-dimensionless number that describes the temperature rate of change in the solid compared to the convective heat transfer between solid and fluid.

The General Lumped Capacitance Method is based on a more complex relation and can therefore not be calculated as simple as the Lumped method. Equation (2.22) shows the GLCM equation valid only for an infinite cylinder.

$$\frac{T_1 - T_2}{T_2 - T_\infty} = C_1 e^{-\zeta_1^2 Fo} J_0(\zeta_1 r^*) \tag{2.22}$$

Were C_1, ζ_1 and J_0 are constants obtained from tables, r^* is the non dimensional radius from the cylinder centreline, i.e. $r^* = 0$ defines the centreline and $r^* = 1$ the cylinder surface. Fo is the Fourier number. More detail on the Lumped and General Lumped Capacitance method can be found in [5].

2.4 Heat treatment processes

The reason for performing a heat treatment process as a part of the manufacturing of a component is that one likes to alter the material properties on a molecular level. Typically the process increases the material temperature, allowing molecules to move through diffusion, and then decreasing the temperature to get the right properties such as grain size and material phases.
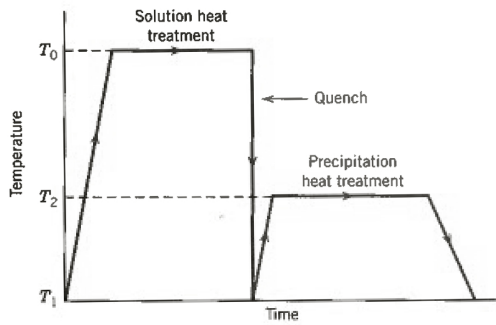
2.4.1 Precipitation hardening

Precipitation hardening is a two step heat treatment process [1] that hardens the material by forming small uniformly dispersed particles of a second phase within the original material phase. This is obtained in a two step process shown in figure 2.1a. For simplicity a hypothetical two phase material is used to describe this process. The hypothetical phase diagram is shown in figure 2.1b.

The first step is called solution heat treatment which by increasing the material temperature to T_0, and hold it there, allowing atoms to diffuse and phase β to dissolve leaving only a single α-phase solid solution left. When the material consists of only the α phase the material is rapidly cooled down to T_1. This stops molecular diffusion leaving the α-phase in a non-equilibrium state with supersaturated B atoms.

The second part of the process is called precipitation heat treatment which by elevating the material temperature to T_2 creates, in a controlled way, small uniformly dispersed β particles within the otherwise supersaturated α phase. Finally the temperature is lowered again to stop the process.

The mechanism of hardening is a phenomenon that occurs due to that the ordinary α phase are reinforced with a large number of small β particles. The β particles acts as movement barriers for dislocations resulting in an increase of yield stress. It is therefore important that there are enough particles dispersed within the α phase and that there are not too large so that the dislocations are not able to move too much.

(a) Material temperature during precipitation hardening
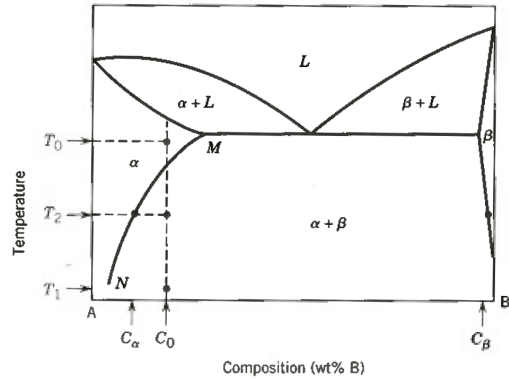
(b) Hypothetical phase diagram

3 Method

The project was divided into two parts. The first one, a pre-study, verifies and investigates CFD tools and heat transfer phenomenas for heat treatment conditions. The purpose of the pre-study was to obtain a deeper understanding of the problem as well as to assess how well CFD tools predicts heat transfer for different flow patterns. The second and main part of the project was then to use this knowledge to simulate the heat treatment process, first for a simplified 2D model and second for a 3D sector.

3.1 Case study

Since there are a large number of cases and sub-cases that have been studied and the general work progress have been quite similar throughout the project this section describes the general approach for all case studies.

The case study consist of a number of steps. First the case need to be defined which was accomplished through discussion with the project supervisors. The case definition included case purpose, fluid domain and a description of what would be studied. Once the case definition was obtained a domain was created according to the definition. Second a computational mesh was made using the software ANSYS Workbench or in some cases, ANSYS IcemCFD. The computational mesh had to fulfil the design practice criterias used by Volvo Aero. These criterias involved requirements on among others cell quality, aspect ratio and growth rate. However the criterias used by Volvo Aero are very similar to commonly used best practice criterias for RANS simulations. Since the heat transfer problems are very dependent on the flow pattern, it is important that the boundary layer is properly resolved with the first layer cell height less than $y+ \leq 1$. The $y+$ value however is velocity dependent which means that the case have to be solved before the $y+$ value can be set. Due to this some iterations were made to obtain a good computational mesh.

With the final mesh obtained the case could be solved using ANSYS Fluent and iterated until both residuals and important parameters such as the wall heat flux had converged, i.e. when the parameters magnitude were

low and had levelled out. After this the results where analysed and compared to correlations or experimental data.

3.2   Pre-study

The pre-study consisted of three cases, each with its own purpose. The three cases are shown in the list below.

- Flow past flat plate

- Flow through a ribbed channel

- Cylinder in cross flow

The flat plate case had the purpose of validating CFD tools for large flat areas such as the inner and outer walls of both hub and shroud. The case were also utilised to study different physical phenomenas such as buoyancy and radiation effects.

The ribbed channel case is based on experiments made by Zahra Ghorbani-Tari [4]. The purpose of this study was to investigate the heat transfer behaviour in highly turbulent areas such as for example behind a flange.

The last pre-study case is the cylinder in cross flow. The purpose was to study fluid-solid coupled heat transfer and compare it to analytical expressions. In excess of fluid-solid coupling the case was utilised in order to evaluate the results if it was solved quasi-transient, solving only the energy equation with a predetermined flow field.

3.2.1   Flat plate

The flat plate case was divided into several sub-cases to be able to study the affect of heat transfer phenomenas individually. The first case studied the heat transfer due to convection for two Reynolds number, approximately 4×10^3 and 12×10^3. The second sub case studies heat transfer due to buoyancy effects, i.e. heat transfer induced by density differences near a heated wall. The next sub-case combines the two previous sub-cases with counter-acting forced and free convection. The last sub case was made to evaluate the impact of radiation from a wall next to the original one with a temperature difference of 100 K.

The flat plate domain is quite simple. It consists of an inlet at the bottom, outlet at the top and a 225 mm no slip wall to the left. The total height is 3 times the wall height, $3 \times 225mm$. The wall is set as the middle part of the left boundary. The domain width is 320 mm and corresponds to the tangential distance between two of the struts connecting the TRS hub to the outer casing. Figure 3.1 shows the flat plate domain. The boundary conditions used are presented in the list below. The inlet gauge pressure was iterated in order to achieve correct Reynolds numbers, $Re \approx 4e3$ and $12e3$.
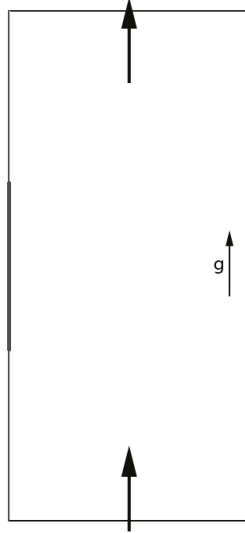
Figure 3.1: Flat plate geometry

- Pressure inlet

  - Gauge pressure (total): 0.19 Pa ($Re \approx 4e3$)
  - Gauge pressure (total): 1.623 Pa ($Re \approx 12e3$)
  - Temperature (total): 700 K
  - Turbulent intensity: 5%
  - Turbulent length-scale: 0.01 m

- Pressure outlet

  - Gauge pressure (static): 0.00 Pa

- Wall

  - No slip
  - Temperature: 800 K

For the last case, where radiation were studied, an additional wall was included. However since only the radiative contribution was of interest, and no effort was made to improve the computational mesh for an additional wall, the boundary condition was implemented with slip condition. The wall temperature implemented with the same temperature as the inlet flow temperature, i.e. 700 K, also both walls had an emissivity of 0.95.

The case was solved both with a laminar solver and the SST k-ω turbulence model. As radiation model the Surface-to-surface model in ANSYS Fluent were used with a Ray tracing method for calculating view factors.

The post-processing consisted of comparison between calculated HTC and Nusselt numbers and well known correlations [5]. For forced convection the correlations are shown in equations (3.1) and (3.2), the first one describing laminar flow and the second turbulent flow.

$$Nu_x = 0.332 Re_x^{1/2} Pr^{1/3} \tag{3.1}$$

$$Nu_x = 0.0293 Re_x^{4/5} Pr^{1/3} \tag{3.2}$$

For sub-cases including buoyancy effects the free convection correlations used were (3.3) and (3.4). The first one valid for $Ra_L \lesssim 10^9$ and corresponds to laminar flow. The second correlation is valid for the entire range of Ra_L however not as good as the previous one for laminar conditions.

$$Nu_x = 0.68 + \frac{0.670 Ra_x^{1/4}}{\left[1 + (0.492/Pr)^{9/16}\right]^{4/9}} \tag{3.3}$$

$$Nu_x = \left[0.825 + \frac{0.387 Ra_x^{1/6}}{\left[1 + (0.492/Pr)^{9/16}\right]^{8/27}}\right]^2 \tag{3.4}$$

The last case was compared to the calculated radiative heat flux obtained by equation (3.5)

$$q''_{rad} = \varepsilon F \sigma (T_w^4 - T_{sur}^4) \tag{3.5}$$

Where F is the view factor that states how large part of the radiation that reach the other wall and was computed according to equation (3.6)

$$F = \frac{([W_i + W_j]^2 + 4)^{0.5} - ([W_i/W_j]^2 + 4)^{0.5}}{2W_i} \tag{3.6}$$

3.2.2 Ribbed channel

The ribbed channel case evaluate heat transfer between the ribs of a ribbed channel. The case consisted of one long channel with an interchangeable test area. The channel could therefor be used to test different rib setups. All rib setups were tested during three different Reynold numbers, based on the hydraulic diameter ($D_h = 128\,mm$) of the real channel, $Re_{D_h} = 57,000$, $89,000$ and $127,000$. A smooth channel was used as reference case for the ribbed channel cases and to obtain boundary conditions for the subdomain where the ribbed channels were evaluated.

The dimensions of the complete channel was $5\,m$ long, $0.08\,m$ high and $0.32\,m$ wide. It consisted of three parts. The first one, a $3.25\,m$ long channel, called the inlet region, with the purpose of generating a fully developed turbulent channel flow. The next part, a $0.5\,m$ long test section where the heat flux was measured. The last part of the channel, the outlet section, was $1.25\,m$ long and used, during simulation, to measure the heat flux further down in the channel and study the repetitiveness of the flow. The ribbed section had five 10x10 mm ribs placed with the pitch of 100, 200, or 300 mm, creating rib pitch-to-height ratio of $p/e = 10, 20$ and 30. Figure 3.2 shows the domain used for the smooth channel.
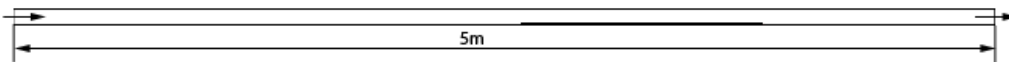

Figure 3.2: Channel domain

The subdomain used for the ribbed cases was 1.75 m long with an inlet section of 0.5 m. However in contrast to the experiments where just the test section was heated, in this case also the outlet part of the channel was heated in order not only to study the turbulence effect of the first ribs but also how it evolves further down in the channel. Figure 3.3 shows the p/e = 20 domain. The turbulence models used for these cases where SST k-ω and
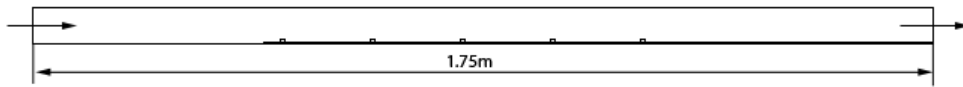

Figure 3.3: Rib domain, p/e = 20

Realisable k-ε.

The boundary conditions used for the simulations are presented in the list below

- Mass flow inlet

  - Mass flow: 0.6567, 1.01991 and 1.45613 kg/s

  - Temperature (total): 295 K

  - Turbulent intensity: 0

  - Turbulent length-scale: 0.128 m

- Walls (Ceiling, inlet bottom wall and ribs)

  - No slip

  - Adiabatic

- Heated Wall

  - No slip

  - Heat flux: 800 W/m^2

- Pressure outlet

  - Pressure (static): 101325 Pa

The correlation used in this case was the Dittus-Boelter correlation for internal turbulent flow [5] given by

$$h = \frac{k_w}{D_H} Nu \tag{3.7}$$

3.2.3 Cylinder in cross flow

The cylinder in cross flow had the purpose of verifying heat transfer and evaluate fluid-solid coupling and compare it to the Lumped, LCM, and General Lumped Capacitance Method, GLCM, explained in the theory section.

To be able to compare the results with both the LCM and GLCM the fluid flow had to be such that on one hand the cylinder temperature is relatively even and on the other hand very uneven, i.e. the temperature gradients should be in the first case low and second large. Therefore two Biot numbers, $Bi = 0.1$ and 8.71, were chosen to fulfil this constraint.

The domain was 0.5 m long and 0.25 m wide with a cylinder of 25 mm in diameter located 200 mm downstream of the inlet as shown in figure 3.4.
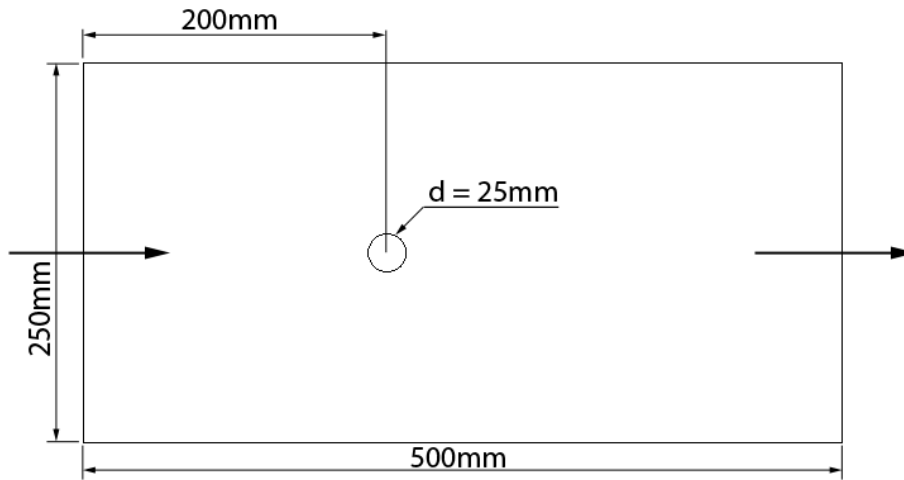
Figure 3.4: Cylinder domain

The boundary conditions are presented in the list below.

- Velocity inlet

    - Velocity: 0.0012 m/s ($Bi = 0.1$)
    - Velocity: 4.333 m/s ($Bi = 8.71$)
    - Temperature: 300 K

- Pressure outlet

    - Pressure: 101325 Pa

- Cylinder wall

    - No slip
    - Thermally coupled with the solid

When these cases were solved the utilised turbulence model was the SST k-ω. However for the quasi-transient simulations where only the energy equation was solved for. The governing flow equations were only used to obtain a representable flow field. The working media utilised in this case was water,

in order to obtain reasonable flow conditions, instead of air or argon as in all other cases.

The cylinder material properties are typical for nickel based alloys and are listed in table 3.1

Table 3.1: Cylinder material properties

Thermal conductivity	Specific heat	Density
20 $W/(m-K)$	871 $J/(kg-K)$	2719 kg/m^3

3.3 Main study

The purpose of the main study was to simulate a part of the heat treatment process for a specific component and compare the results to measurements performed during the manufacturing process. This was first executed on a simplified axi-symmetric 2D model. The 2D model where run for several cases with different physics and time steps in order to evaluate how much the model could be simplified without compromising the results too much.

Lastly a 3D model was supposed to be simulated in order to combine the obtained knowledge and evaluate if reasonable simulations of the heat treatment process are possible to perform.

3.3.1 2D axi-symmetric oven model

The axi-symmetric 2D model was used to simulate several sub-cases, each with different settings. As a reference case an ordinary transient simulation with only forced convection heat transfer was used. To this reference case, buoyancy and radiation were added individually in order to investigate their importance for the overall heat transfer. The last sub case included both buoyancy and radiation to review their combined effects. The reference case was also used to check the time step independence. In total, four different time steps were checked, ranging from $\Delta t = 0.05$ s to 1 s. The last case, included both gravity and radiation. The case was run several times with different wall emissivity settings. The wall emissivity was set individually to 0.25, 0.5 and 0.75 to evaluate whether it was possible or not to tweak the emissivity so that the simulated temperature would agree better with the measured ones.

The axi-symmetric 2D model domain is shown in figure 3.5. It consists of a bottom wall with three inlets, a right wall with seven inlets, top with two outlets and the left axi-symmetric boundary. Inside are a simplified 2D model of the Turbine Rear Structure and the graphite plate that it is standing on during the heat treatment process.

The boundary conditions used are presented in the list below. The real oven have a constant volume flow during the process. However since that kind of boundary condition is not implemented in ANSYS Fluent a time dependent mass flow condition according to the inlet temperature drop was utilised. The total inlet mass flow rate and temperature were set by polynomials stated in equations (3.8) and (3.9). These polynomials where obtained from
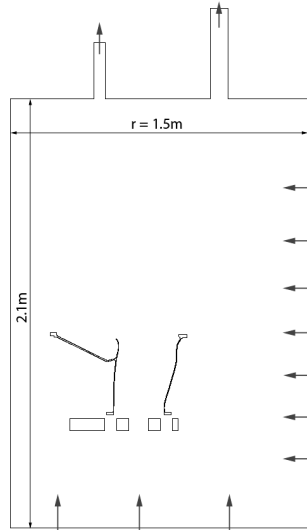
Figure 3.5: 2D model domain

fitting polynomials to measurements of the inlet fluid temperature during manufacturing.

$$\dot{m}_{in} = -2.8970 \times 10^{-21} t^6 + 5.9088 \times 10^{-17} t^5 - 4.2707 \times 10^{-13} t^4 +$$
$$1.2799 \times 10^{-9} t^3 - 2.1193 \times 10^{-6} t^2 + 9.8433 \times 10^{-3} t + 9.5990 \quad (3.8)$$

$$T_{in} = 1.0610 \times 10^{-19} t^6 - 2.6944 \times 10^{-15} t^5 + 2.7666 \times 10^{-11} t^4 -$$
$$1.4970 \times 10^{-7} t^3 + 4.7227 \times 10^{-7} t^2 - 9.0645 \times 10^{-1} t + 1.2270 \times 10^3 \quad (3.9)$$

- Mass flow inlets

    - Mass flow, (3.8), the inlet mass flow was divided equally between the bottom and side wall
    - Temperature, (3.9)
    - Turbulent intensity: 10 %
    - Turbulent length-scale: Diameter of the inlets

- Pressure outlets

    - Pressure: 2.1 *bar*

- Oven walls

    - No slip
    - Temperature, (3.9)

- TRS and plate walls

    - No slip
    - Thermally coupled with solid

3.3.2   3D oven sector

The 3D sector case was supposed to evaluate how 3D effects would affect the flow and heat transfer patterns. The TRS consists of 13 relatively symmetric sectors, a few of them have mounting parts that adds complexity to the heat treatment problem. However local geometry differences lies outside the scope of this thesis and therefore not included in the 3D sector model. Figure 3.6 shows a 3D view over the domain. The 3D sector case was the last case and
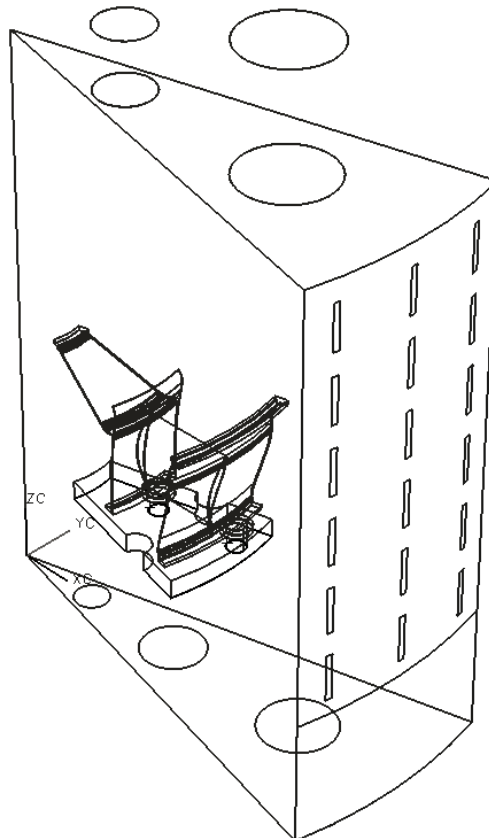
Figure 3.6: 3D sector domain

due to lack of time and the domain complexity the case could not be finished.

4   Results and Discussion

This chapter presents and discuss the results obtained from all cases within this project. More details about the results in terms of plots and graphs can be found in appendix A-D.

4.1   Flat plate

In this section the results for the flat plate case is presented and discussed, beginning with forced and free convection. Below some figures of Nusselt number and heat transfer coefficient are presented. More figures of flow and heat transfer patterns can be found in appendix A.

4.1.1 Convection

During this subsection the result of simulations made of forced and free convection are presented individually.

First the forced convection case was simulated. Figure 4.1 shows the local Nusselt number for two different Reynolds number cases and the flat plate heat transfer correlations for both laminar and turbulent flow. It is believed that due to inlets and domain irregularities the conditions of the heat treatment process have low turbulence intensity. This would imply that a turbulence model is needed, despite the fact that the Reynolds number in both cases are well below the transition point. As seen in the figures both the laminar solver and the SST k-ω turbulence model predicts the laminar correlation very well. However at the end of the plate one can see that the simulations over predicts the heat transfer. This is believed to depend on wall end effects that the correlations does not take into consideration.

(a) $Re = 4300$ (b) $Re = 12800$
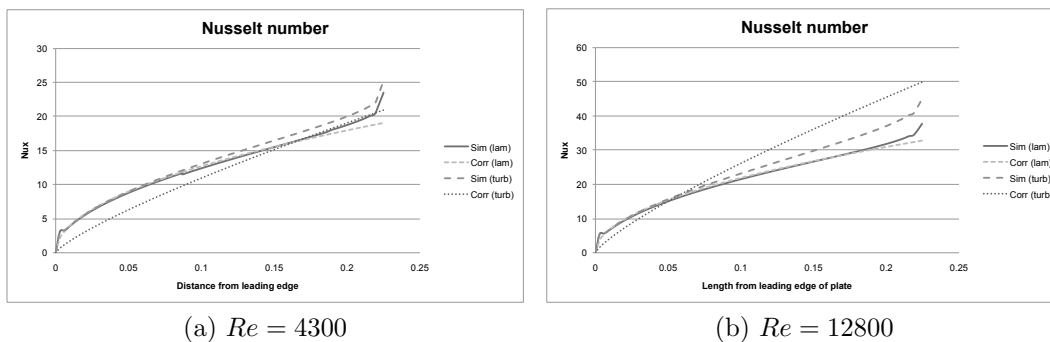
Figure 4.1: Nusselt number variation for forced convection over flat plate

The free convection Nusselt number comparison can be seen in figure 4.2. Also in this case the simulations with both the laminar solver and the turbulence model predicts the heat transfer very well. The SST k-ω model over predicts the heat transfer slightly which indicate that there are some problems when using a turbulence model for a laminar case. However the result that the turbulence model predict is quite close to the correlation and the error is acceptable. It is also clear that the turbulent correlation is not valid for the present conditions.
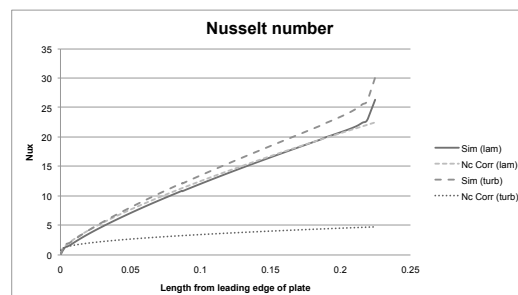
Figure 4.2: Nusselt number variation for free convection case

4.1.2 Mixed convection

The mixed convection case studies the combined counter acting convection problem of both forced and free convection. The difference is that now the buoyancy is counter acting the induced flow. The heat transfer for the first low Reynolds number case is shown in figure 4.3a. It shows that the predicted heat transfer rate does not agree at all with any of the correlations. The reason for this can be seen in figure 4.4 were it is clear that the temperature boundary layer is not smooth as in the forced convection case. It is the buoyancy effect that prevents the heat transfer rate for great parts of the plate. The second case with a higher Reynolds number is shown in figure 4.3b. It shows that the heat transfer agrees well with the laminar correlation for forced convection. This implies that the buoyancy have no impact when the induced flow is strong enough. Another way of describing this is by the ratio between free and forced convection heat transfer where the first case have a ratio of approximately 0.5 and the second case approximately 0.05.

| (a) $Re = 4300$ | (b) $Re = 12800$ |
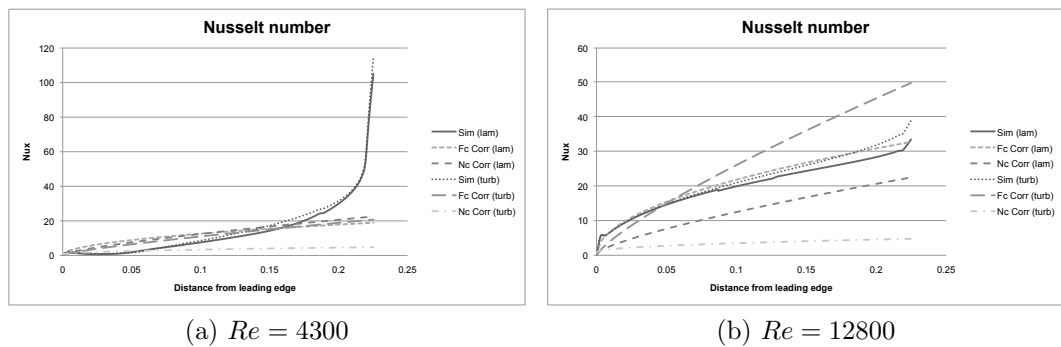
Figure 4.3: Nusselt number variation for mixed counter acting convection
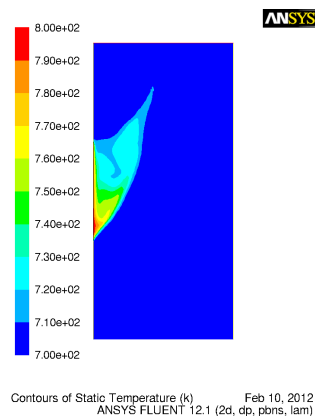
Figure 4.4: Temperature variation for the counter acting mixed convection flow

4.1.3 Radiation

The last flat plate case evaluates radiative heat transfer from an opposite wall. Since radiation is little affected by the working media the flow simulations were made as simple as possible, i.e. the first low Reynolds number

forced convection case with a laminar solver was used. The radiation model used was a surface-to-surface model which assumes that the working media does not affect the radiative heat transfer at all. The heat transfer rate is shown in figure 4.5 and it shows that for these conditions the radiative heat transfer have a large impact on the overall heat transfer rate. However the amount of radiative heat transfer does not agree with the theoretical value and unfortunately the reason for this difference could not be found.
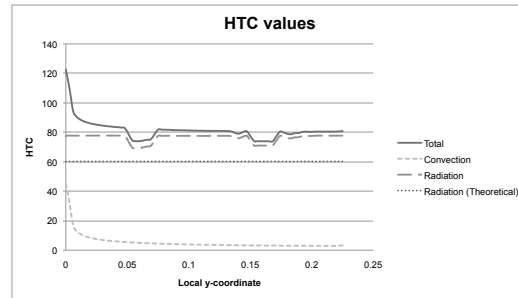
Figure 4.5: HTC value for convection and radiation heat flux

4.2 Ribbed channel

This sub section presents the result of the ribbed channel case. It consists of four sub-cases, one long smooth channel and three ribbed channels with different rib pitches. Figures of flow patterns can be found in appendix B

4.2.1 Long smooth channel

In figure 4.6 the comparison between two turbulence models and experimental results are presented. The results are also compared to the Dittus-Boelter correlation. Both the Realisable k-ε and SST k-ω predicts the heat transfer rate for a smooth channel very well and both the simulated heat transfer rate and the experiments approaches the Dittus-Boelter correlation in the same way indicating that the experimental results are trustworthy. Figure
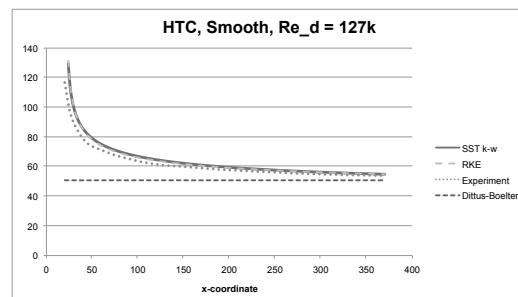
Figure 4.6: HTC comparison between turb. models and experiment

4.6 shows the results for the highest Reynolds number simulated. Result for the lower Reynolds numbers have similar results and can be found in appendix B

4.2.2 Ribbed channel

In figure 4.7 the heat transfer coefficient are shown for each rib pitch case. The Reynolds number, that is shown is the highest that have been investigated and shown here because it is the most extreme flow case. The figures show that even though the mesh resolves the boundary layer the simulations are still not able to predict the heat transfer rate. This is believed to be caused by the turbulence models and their shortcomings for predicting flow fields in areas with high turbulent intensity.

(a) $p/e = 10$, $Re = 127000$

(b) $p/e = 30$, $Re = 127000$

(c) $p/e = 30$, $Re = 127000$
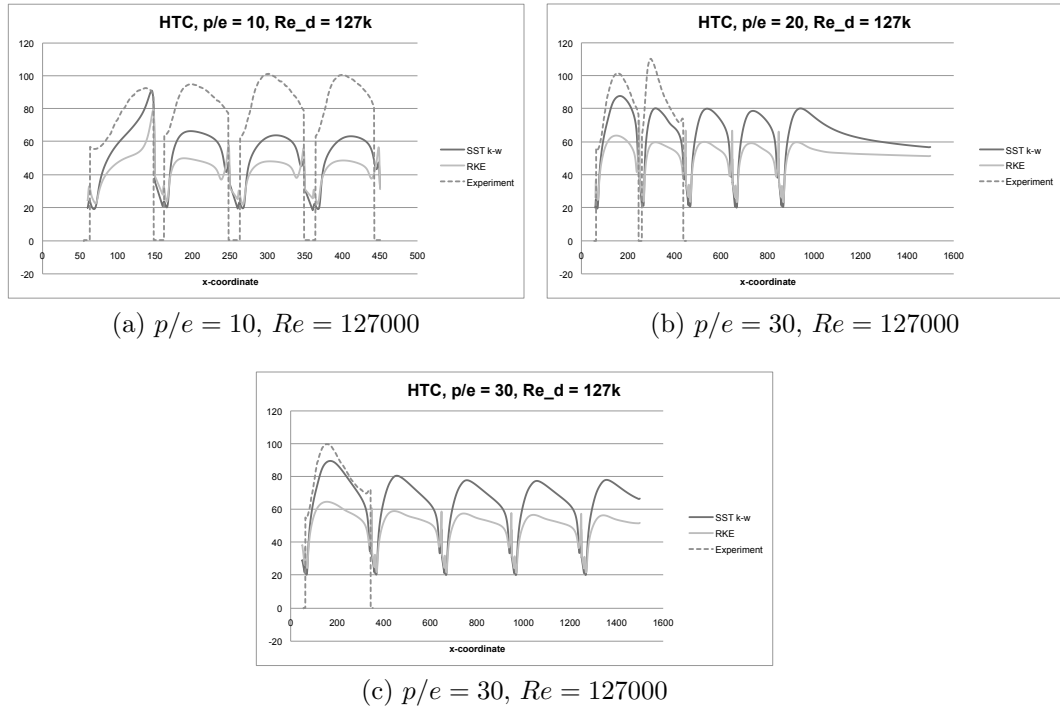
Figure 4.7: HTC for ribbed cases

Table 4.1 presents the difference between experimentally obtained and simulated HTC-values for the first inter rib area.

Table 4.1: Comparison of HTC-value between experiments and simulations for the first inter rib area

	$Re = 57,000$	$Re = 89,000$	$Re = 127,000$
p/e = 10			
Rke	26.4%	25.0%	37.8%
SST k-ω	17.9%	13.0%	23.8%
p/e = 20			
Rke	36.8%	31.6%	35.7%
SST k-ω	23.9%	21.1%	17.4%
p/e = 30			
Rke	35.4%	37.1%	31.9%
SST k-ω	21.3%	20.7%	13.2%

For the ribbed cases, the response using wall functions were also investigated. The heat transfer coefficients, simulated with wall functions are shown in figure 4.8a. The figure shows that wall functions gives a much better heat transfer agreement then a resolved mesh, for both the Realisable k-ε and SST k-ω model. This was very unexpected since wall functions should, in general, give a less accurate result than a well resolved wall boundary layer. The explanation for this is that the wall function simulation did not capture the recirculation zones in a correct way resulting in a two-wrongs-make-it-right situation. It is however very doubtful that wall functions will work for other cases.
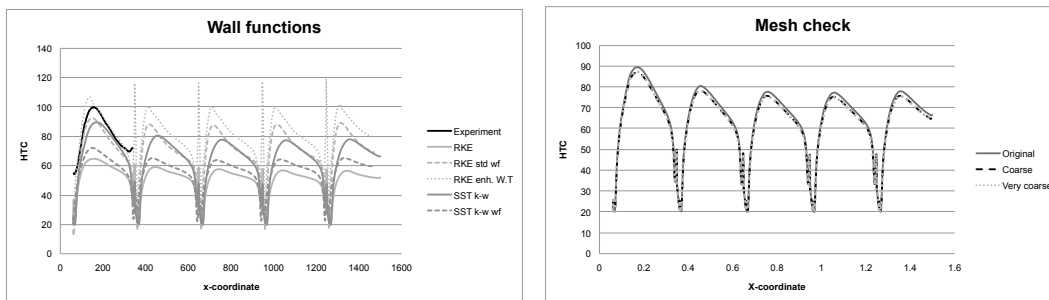
(a) Heat flux simulated using wall functions   (b) HTC values of mesh independence

Last, a mesh independence check was made. The mesh statistics are presented in table 4.2. Figure 4.8b shows that despite decreasing the mesh size by half the results are barely affected which indicates that there is mesh independence.

Table 4.2: Mesh size

Mesh	No. of cells
Original	240,000
Coarse	180,000
Very coarse	140,000

4.3   Cylinder in cross flow

The cylinder in cross flow case evaluates several phenomenas. First it evaluates how the HTC value is predicted and compared to the average Nu value over the first 90 degrees of the cylinder wall. Second the case was utilised to evaluate the Lumped and General Lumped capacitance method. Finally the case verifies the effect of running quasi-transient heat transfer simulations instead of ordinary transient ones.

Figure 4.8 shows the local HTC value for the whole cylinder with Biot numbers of 0.1 and 8.71. The figures show that in the first case 4.8a the flow is laminar and attached to the cylinder. There is no clear separation point as for the second case 4.8b. The separation point is shown as a jump in HTC value and is located around 90 degrees.

For comparing the average Nusselt number for the first quarter of a 2D cylinder in cross flow a Volvo Aero specific correlation based on a study

(a) $Bi = 0.1$ (b) $Bi = 8.71$
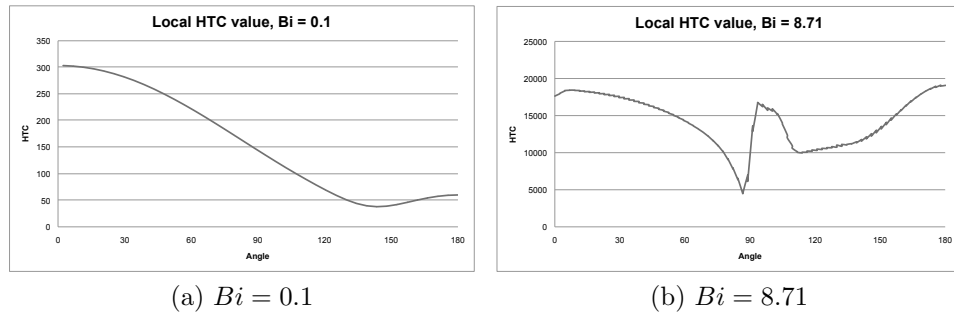
Figure 4.8: Local HTC value

made by Nils Frössling in 1958, [3]. Table 4.3 shows the predicted Nu, the correlation and the error. As seen in the table the errors are very small, less than 5%, which is a prerequisite for the latter studies of LCM and GLCM.

Table 4.3: Nusselt number for different Biot numbers

	$\mathbf{Nu_{Predicted}}$	$\mathbf{Nu_{Frossling}}$	**Error**
Bi = 0.1	6.505	6.440	1.00%
Bi = 8.71	596.2	581.0	2.62%

As mentioned in the theory section the Lumped and General Lumped Capacitance Methods describes the material temperature of the solid, in this case a cylinder. The cylinder in crossflow case is therefore designed to validate two analytical methods for predicting the internal temperature. Figures 4.9a and 4.9c shows the material temperature of the cylinder over time at two locations, at the centre and on the surface of the cylinder. Figures 4.9b and 4.9d shows the internal temperature profiles at different times. These figures show clearly the difference between a high and low Biot number. The high Biot number give very large temperature differences within the material. Therefor the Lumped capacitance method cannot predict the material temperature for this case as shown in figure 4.9c. For a low Biot number however the LCM can be used with just a small resulting error. The LCM assumes a completely uniform temperature which in reality is not true. The GLCM was also used for the same case however due to errors in the hand calculations the GLCM was unable to predict the cylinder temperature. Since the important thing was the LCM, only a limited time where spent on locating this error.

The last thing studied was quasi-transient simulations versus transient heat transfer simulations. The temperature drop for both simulations can be seen in figure 4.9. The quasi-transient results are presented by the orange and lies just on top of the transient simulations which means that for a quite steady flow the quasi-transient simulation agrees very well with the transient results.

(a) Temperature over time, $Bi = 0.1$ (b) Temperature profiles, $Bi = 0.1$

(c) Temperature over time, $Bi = 8.71$ (d) Temperature profiles, $Bi = 8.71$
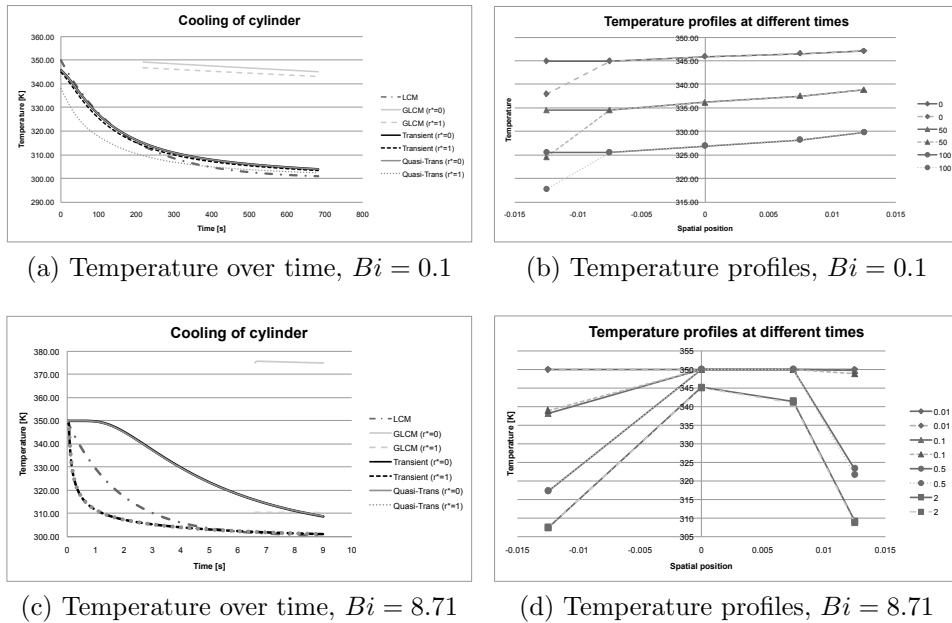
Figure 4.9: Material temp. over time and temperature profiles

4.4 2D axi-symmetric oven model

The 2D axi-symmetric oven model is the first case study within the main part of the project. The results consists of a comparison between simulated and measured surface temperature at eight different locations. These locations are shown here in figure 4.10.
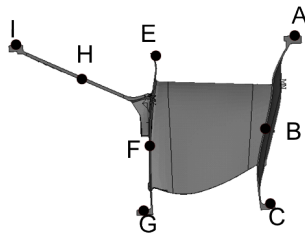
Figure 4.10: Locations of measuring points

Figure 4.11 shows the surface temperature during the first eight minutes of the cooling process. It is clear from the figures that without radiation the required cooling rate cannot be achieved. However these figures does not say much about how buoyancy affects the cooling rate. The two figures 4.11c and 4.11d show however that the overall cooling rate is slightly different. The one including both radiation and gravity have a slightly lower cooling rate than the one considering only the radiation. The reason for this is that there are large recirculation areas surrounding the TRS and the main fluid motion closest to the TRS surface is downwards whereas motion induced by buoyancy is upwards, counter acting the general flow pattern and thereby lowering the heat transfer coefficient slightly.

What also is hard to see on the four figures above is how well the simulations predict the local temperature. Figure 4.12 show, for the convective case including both buoyancy and radiation, the temperature difference between

(a) Convective heat transfer

(b) Convective heat transfer including buoyancy

(c) Convective heat transfer including radiation

(d) Convective heat transfer including buoyancy and radiation
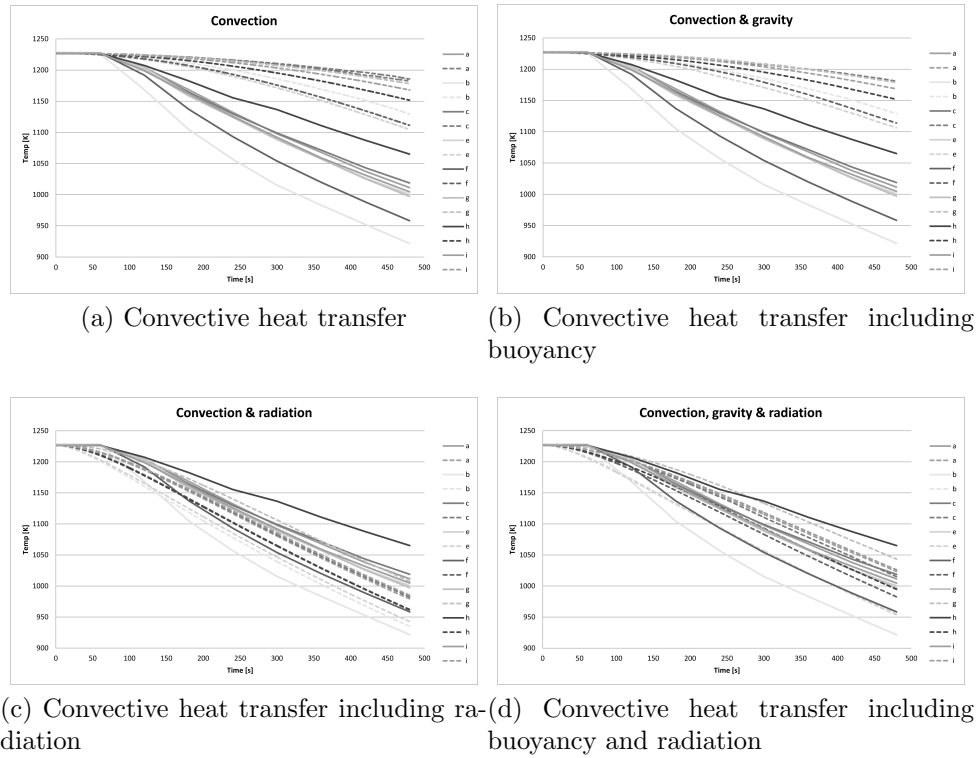
Figure 4.11: Comparison between predicted (dashed) and measured (solid) temperatures

simulated and measured data. It is clear that locally there are great differences between the simulations and the reality. Figure 4.12 where obtained in order to evaluate the radiative heat transfer from the oven floor, ceiling and wall individually. The result from this study was that, by changing the wall emissivity, the local temperature errors could not be decreased enough and the local variations must therefore come from 3D effects.
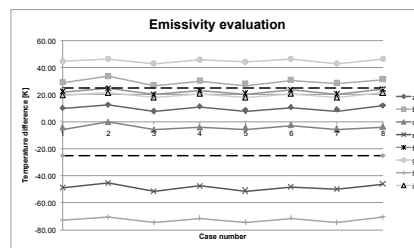
Figure 4.12: Evaluation of wall emissivity to predicted and measured ΔT

Table 4.4: Time step dependence check, errors compared to $\Delta t = 0.05s$

Δ t [s]	a	b	c	e	f	g	h	i
0.05	-	-	-	-	-	-	-	-
0.1	-0.84%	-1.01%	0.09%	0.38%	0.54%	0.08%	0.10%	0.11%
0.5	-1.21%	-0.55%	-1.16%	1.17%	1.01%	-0.01%	0.10%	0.15%
1	-0.93%	-0.47%	-4.22%	-2.24%	3.34%	0.30%	-0.07%	0.43%

5 Conclusions and Recommendations

The thesis purpose was to obtain a deeper knowledge about the heat transfer occurring during the aggressive cooling of the precipitation hardening process of the Turbine Rear Structure. Simulations have shown that for low Reynolds number flow, buoyancy have a significant impact on the heat transfer rate and contributes mainly to local temperature variations. It has also been shown that when simulating the heat treatment process the required cooling rate could not be achieved without radiative heat transfer.

Except getting a deeper understanding of the heat treatment process the project purpose was to evaluate CFD tools, mainly the turbulence models for these types of flows. The results show that the SST k-ω is the preferred turbulence model. This is due to that it predicts the heat flux for highly turbulent areas much better. However, even though the SST k-ω model is better than the Realisable k-ε model it still fails to predict the heat flux in very high turbulent areas to a satisfying level. Therefore one needs to be aware of that the heat flux in these areas might be under predicted.

In the main part of the project a time step dependence check for the 2D axi-symmetric case was made. It showed that the process flow field is quite steady. It is mainly the temperature that changes with time which allows a relatively large time step in the simulations.

Conclusively the studies show that when performing transient simulations of a complex model like the TRS a 3D model should be used. Also, both buoyancy and radiation have to be included. Finally the preferred turbulence model is the SST k-ω model.

At this stage there still are one rather large source of error left that should be sorted out before continuing with the project. This error source is the wall material emissivity. It is unknown and probably temperature dependent. It is therefore recommended to simulate the heating part of the heat transfer process which is performed in "vacuum". Doing so simplifies the problem leaving practically only the radiative heat transfer left which from then the wall emissivity can be found.

References

[1] William D. Callister. *Materials Science and Engineering: An Introduction*. John Wiley & Sons, Inc., seventh edition, 2007.

[2] Lars Davidsson. Fluid mechanics, turbulent flow and trubulence modeling. Technical report, Department of Applied Mechanincs, Chalmers University of Technology, Sweden, 2011.

[3] N. Frössling. Evaporation heat transfer and velocity distribution in 2d and rotationally symmetrical laminar boundar layer flow. *NACA TM 1432*, 1958.

[4] Z. Ghorbani-Tari, B. Sundén, and G. Tanda. Experimental study of convection heat transfer in the entrance region of a rectangular duct with transverse ribs. 2012.

[5] Frank P. Incropera, David P. Dewitt, Theodore L. Bergman, and Adrienne S. Lavine. *Fundamentals of Heat and Mass Transfer*. John Wiley & Sons, Inc., sixth edition, 2007.

[6] F. R. Menter. Two-equation eddy-viscosity turbulence models for engineering applications. *AIAA Journal*, 32(8):1598–1605, 1994.

[7] T.-H. Shih, W. W. Liou, A. Shabbir, and J. Zhu. A new k-ϵ eddy viscosity model for high reynolds number turbulent flows. *Computers Fluids*, 24(3):227–238, 1995.

[8] H K Versteeg and W Malalasekera. *An Introduction to Computational Fluid Dynamics: The Finite Volume Method*. Pearson Education Limit, second edition, 2007.

A Flat plate
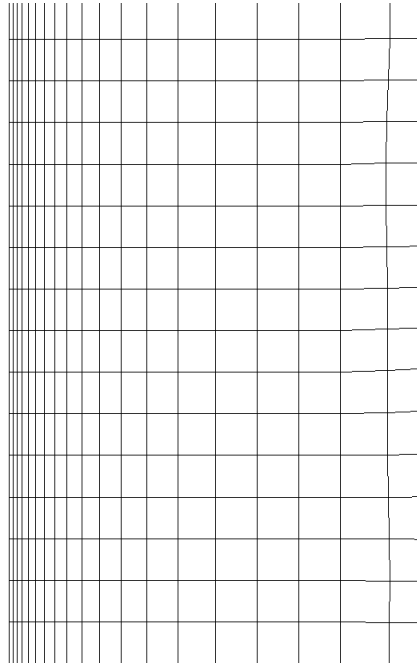
Figure A.1: Resolved mesh used for low Reynolds number case
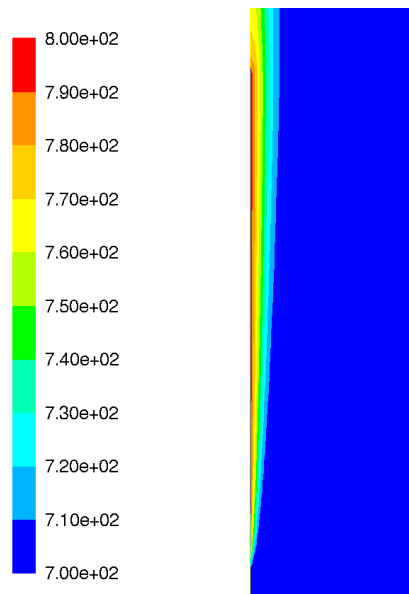
Figure A.2: Static temperature near the heated plate for forced convection case
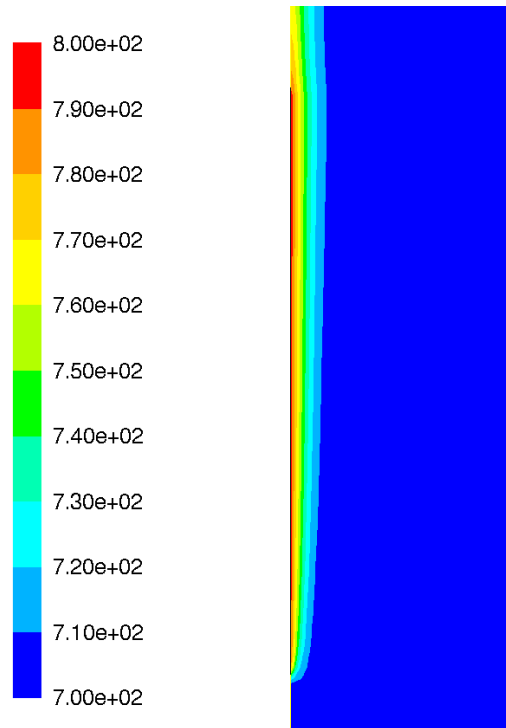
Figure A.3: Static temperature near the heated plate for natural convection case
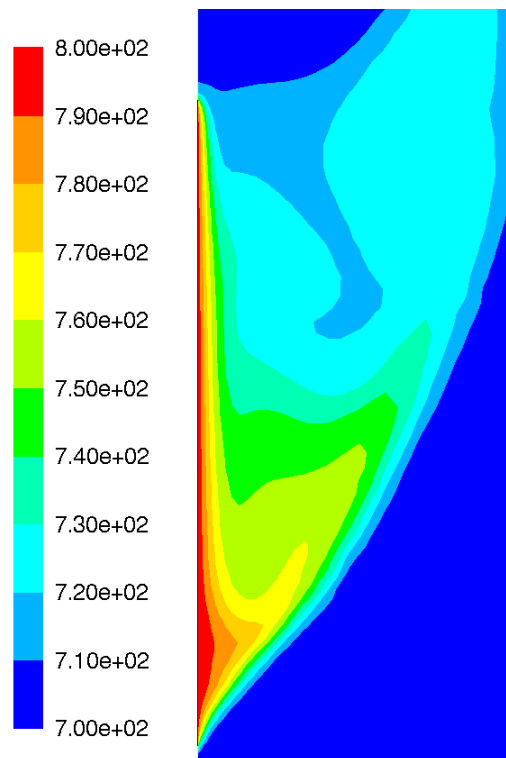
Figure A.4: Static temperature near the heated plate for counteracting mixed convection and low Reynolds number case

B Ribbed channel
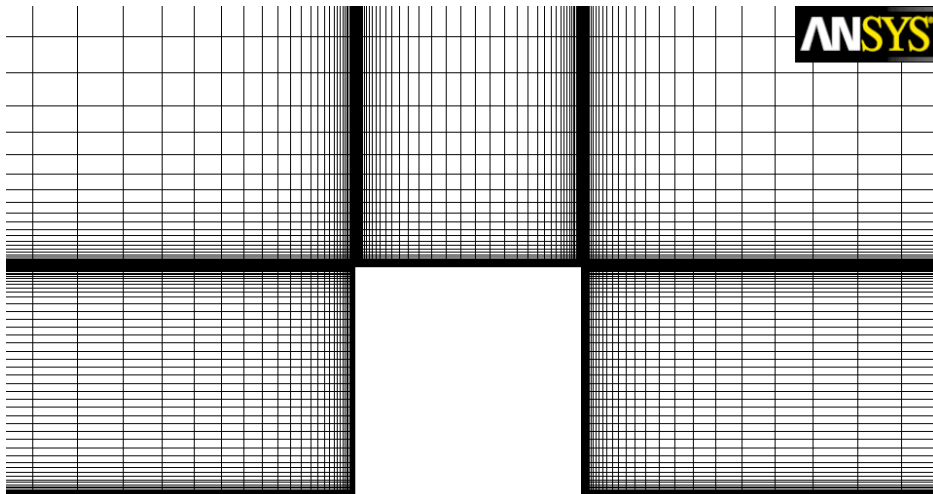
Figure B.1: Mesh around one of the ribs
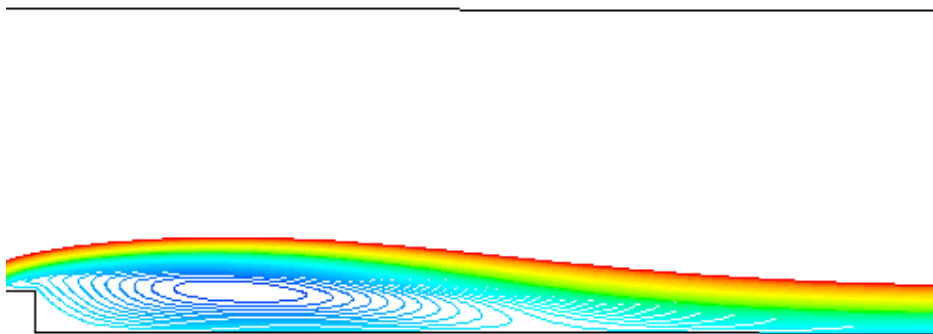
Figure B.2: Stream lines obtained with the SST k-ω model between the first and second ribs for the p/e=30 and $Re_h = 89k$ case
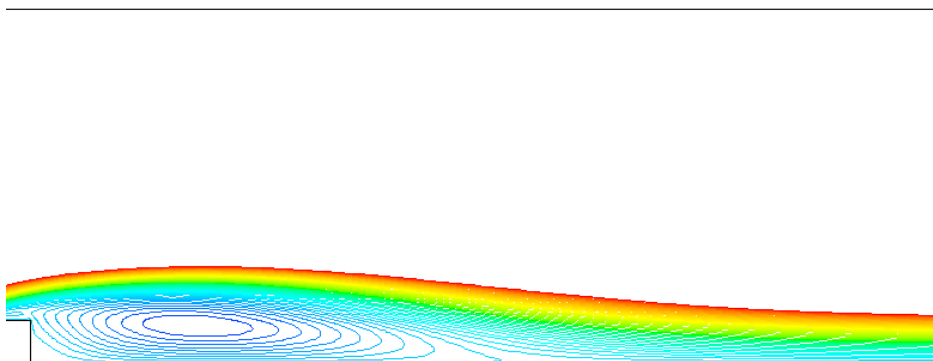
Figure B.3: Stream lines obtained with the realisable k-ε model between the first and second ribs for the p/e=30 and $Re_h = 89k$ case
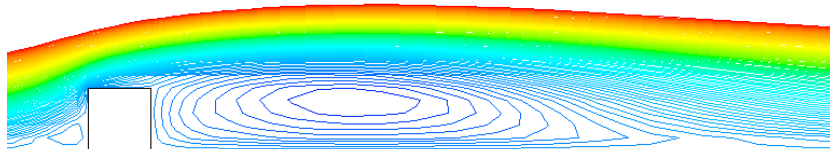
Figure B.4: Stream lines obtained with the realisable k-ε model between the first and second ribs for the p/e=30 and $Re_h = 127k$ case
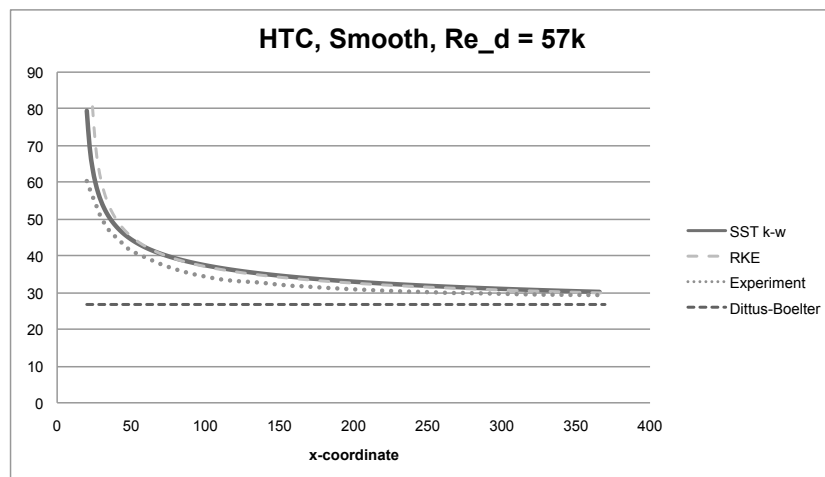
Figure B.5: HTC comparison between turb. models and experiment
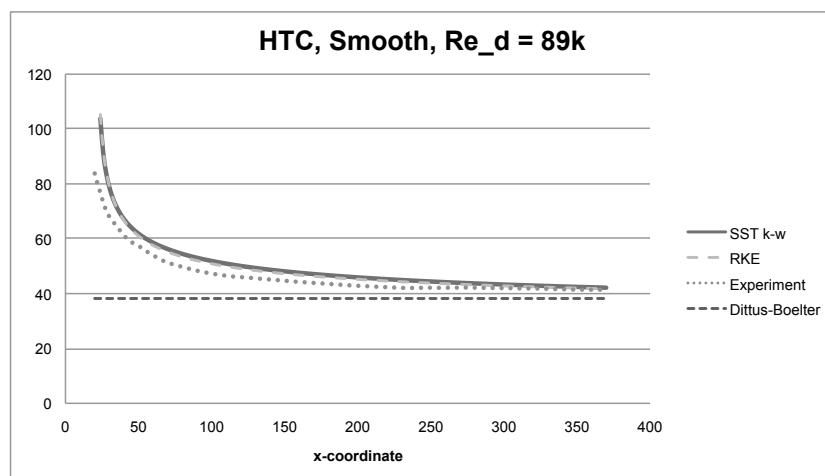
Figure B.6: HTC comparison between turb. models and experiment
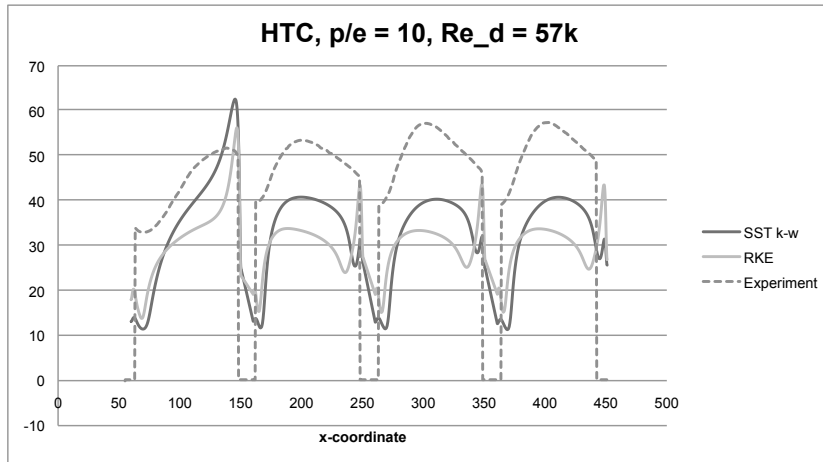
Figure B.7: HTC comparison between turb. models and experiment
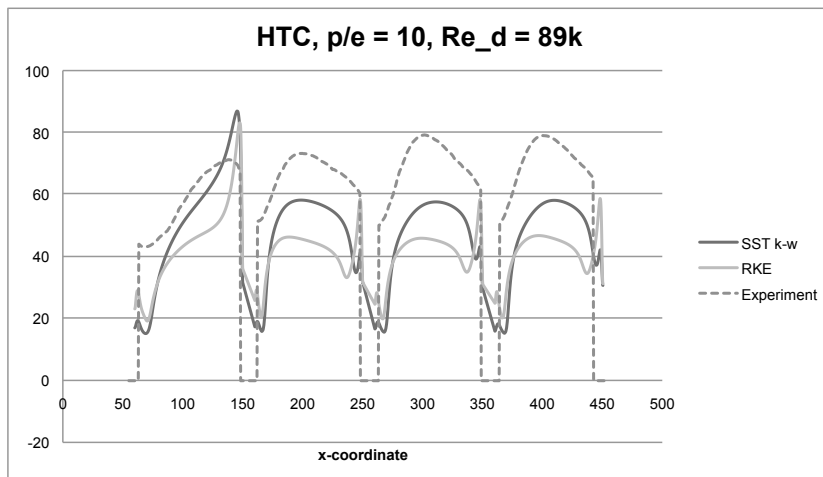
Figure B.8: HTC comparison between turb. models and experiment
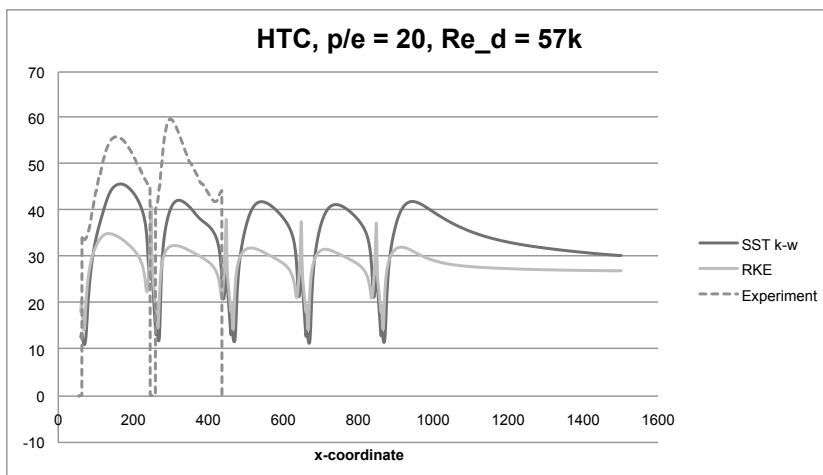
Figure B.9: HTC comparison between turb. models and experiment
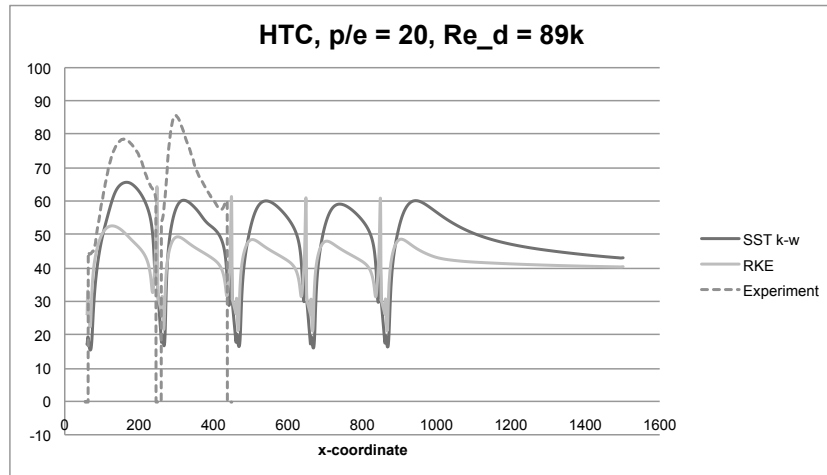
Figure B.10: HTC comparison between turb. models and experiment
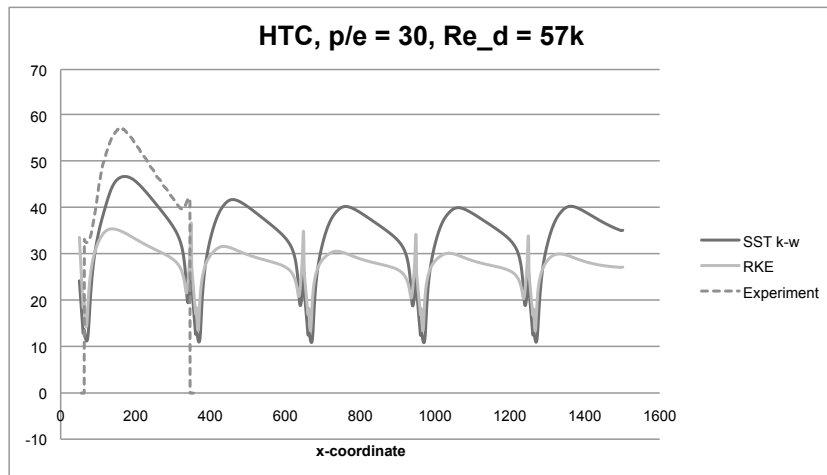
Figure B.11: HTC comparison between turb. models and experiment
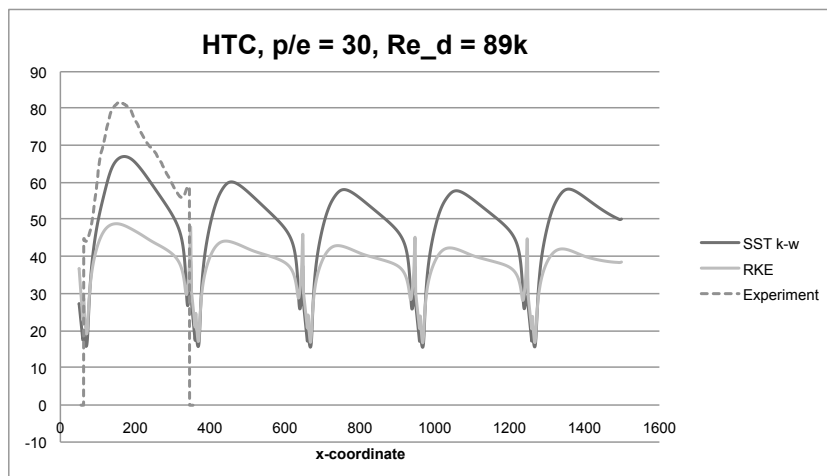
Figure B.12: HTC comparison between turb. models and experiment

C   Cylinder in cross flow
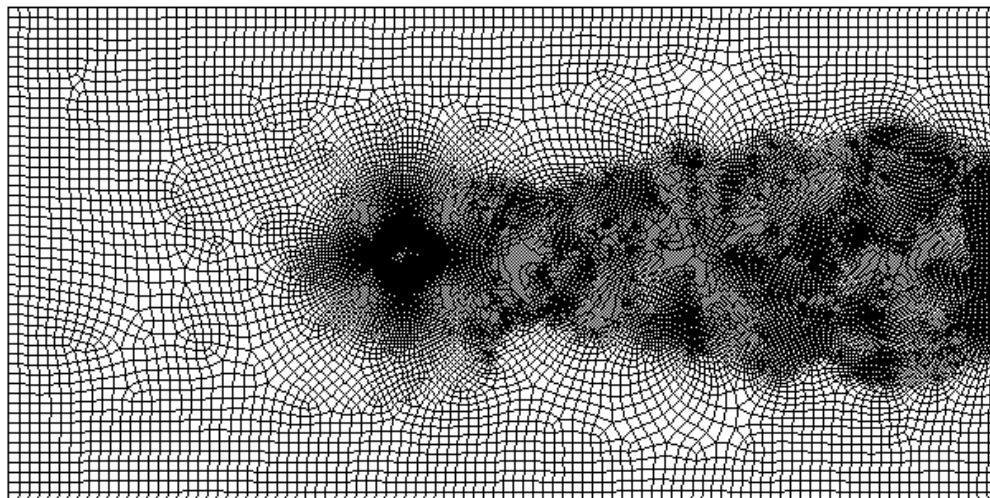
Figure C.1: Fine mesh
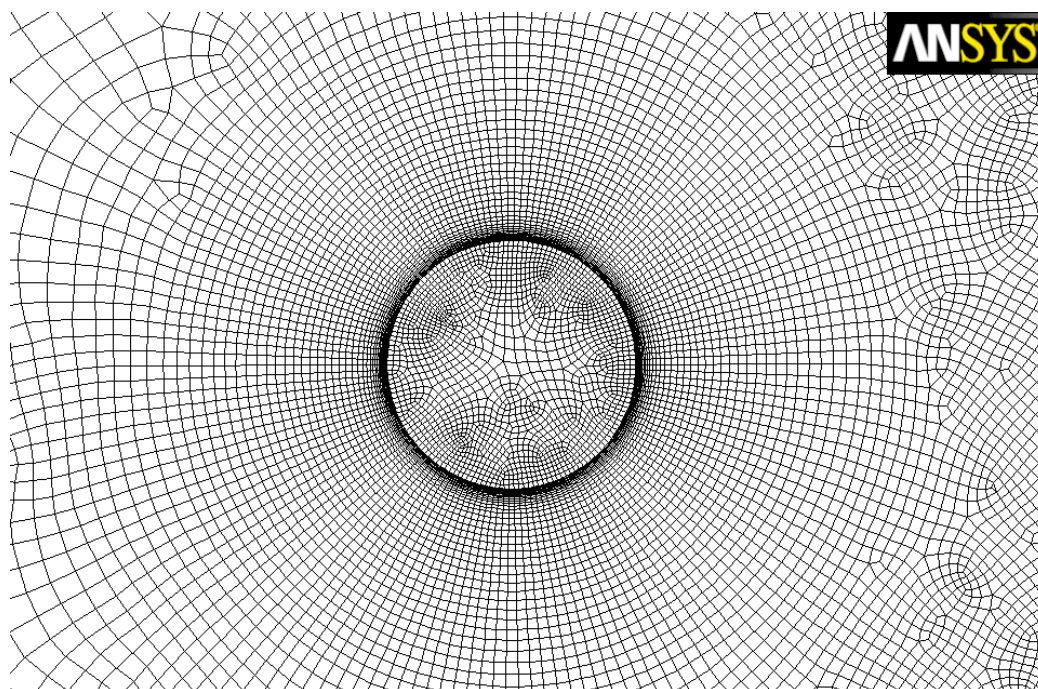
Figure C.2: Close up on mesh around the cylinder
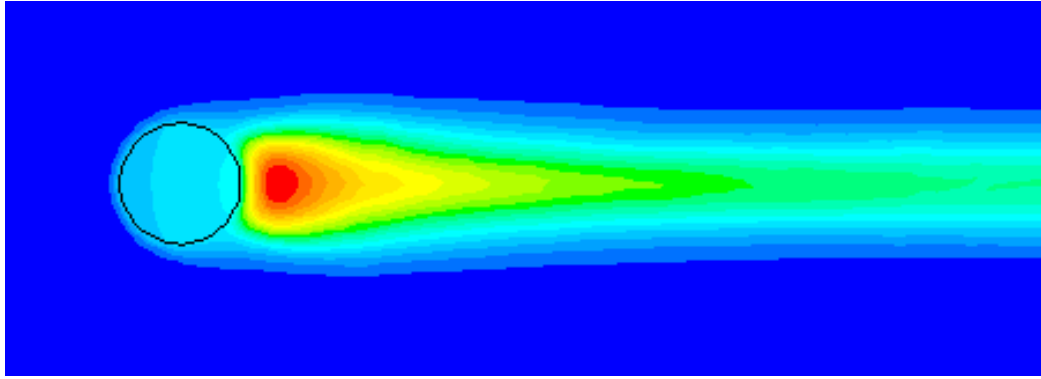
Figure C.3: Temperature for the low Biot number case
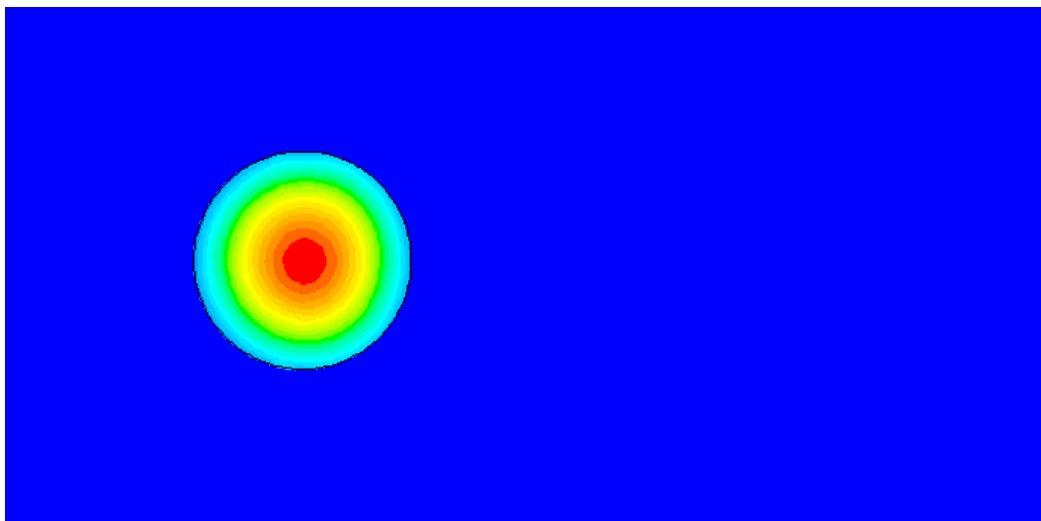
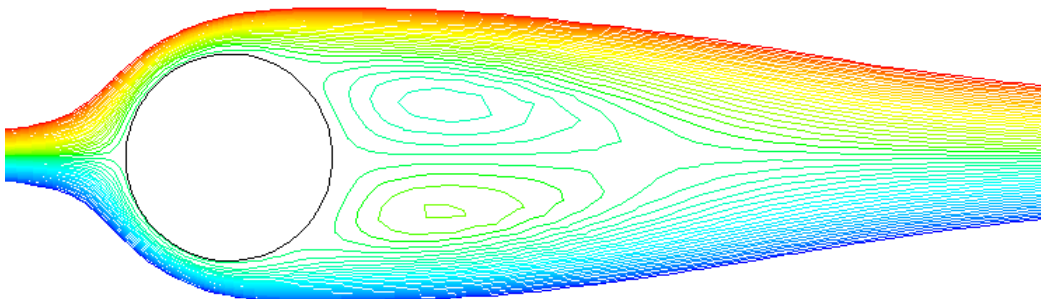Figure C.4: Temperature for the high Biot number case

Figure C.5: Streamlines for the low Biot number case
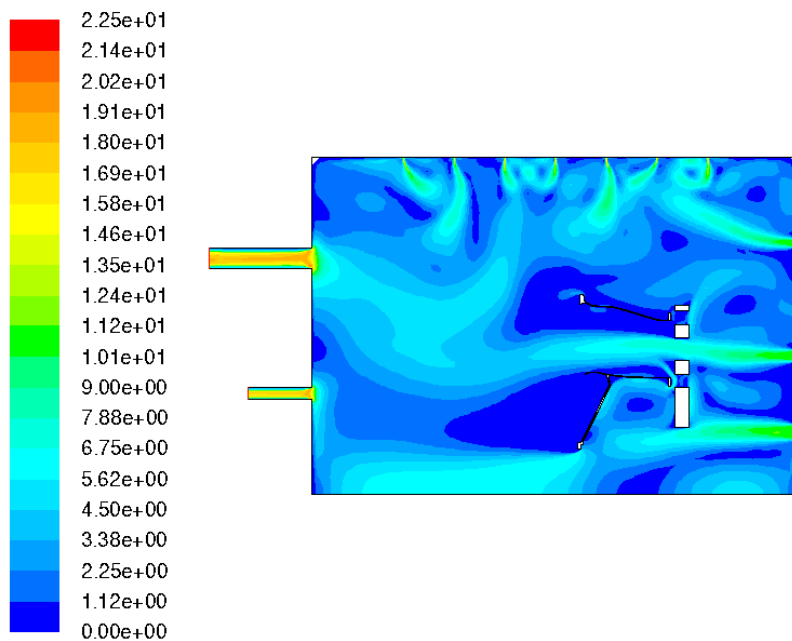
D 2D axi-symmetric oven model

Figure D.1: Velocity magnitude at eight minutes of cooling with both gravity and radiation included
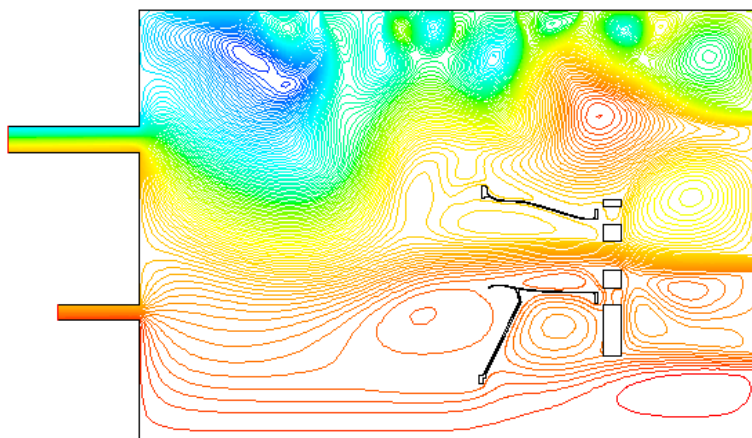

Figure D.2: Stream function at eight minutes of cooling with both gravity and radiation included
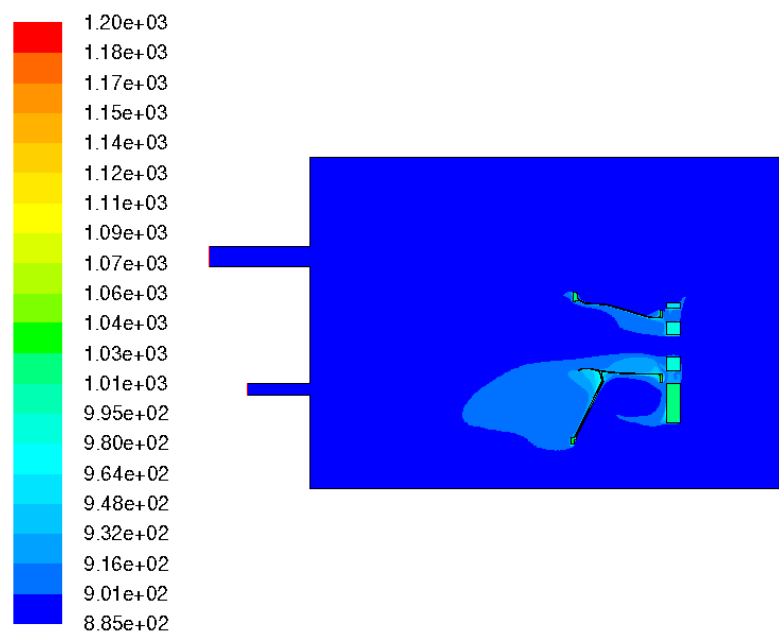
Figure D.3: Static temperature at eight minutes of cooling with both gravity and radiation included